24
Boundary layers

Between the two extremes of sluggish creeping flow at low Reynolds number and lively ideal flow at high, there is a regime in which neither is dominant. At large Reynolds number, the flow will be nearly ideal over most of space, except near solid boundaries where the no-slip condition requires the speed of the fluid to match the speed of the boundary wall. Here will arise transition layers in which the flow velocity changes rapidly from the velocity of the wall to the velocity of the flow in the fluid at large. Boundary layers are typically thin compared to the radius of curvature of the solid walls, and that simplifies the basic equations.

In a boundary layer the character of the flow thus changes from creeping near the boundary to ideal far from it. The most interesting and also most difficult physics characteristically takes place in such transition regions. But humans live out their lives in nearly ideal flows of air and water at Reynolds numbers in the millions with boundary layers only millimeters thick, and are normally not conscious of them. Smaller animals eking out a turbulent existence at the surface of a stone in a river may be much more aware of the vagaries of boundary layer physics which may influence their body shapes and internal layout of organs.

Ludwig Prandtl (1875–1953). *German physicist, often called the father of aerodynamics. Contributed to wing theory, streamlining, compressible subsonic airflow, and turbulence.*

Boundary layers serve to insulate bodies from the ideal flow that surrounds them. They have a "life of their own" and may separate from the solid walls and wander into regions containing only fluid. Detached layers may again split up, creating complicated unsteady patterns of whirls and eddies. Advanced understanding of fluid mechanics begins with the understanding of boundary layers. Systematic boundary layer theory was first advanced by Prandtl in 1904 and has in the 20'th century become a major subtopic of fluid mechanics [50, 51].

In this chapter we shall mainly focus on the theory of incompressible laminar boundary layers without heatflow, and present a semi-empirical discussion of turbulence.

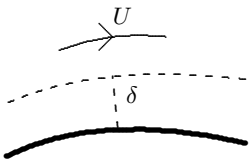

The transition from zero velocity at the wall to the mainstream velocity U mostly takes place in a layer of finite thickness δ.

24.1 Physics of boundary layers

Consider a nearly ideal flow with velocity U along a solid wall at rest. The Reynolds number is as usual calculated as $\mathsf{Re} \approx UL/\nu$ where L is a typical length scale for significant changes in the flow, determined by the geometry of bodies and containers. The no-slip condition requires the velocity to vary from zero right at the wall to U in the flow at large. Under many — but not all— circumstances, this transition will for $\mathsf{Re} \gg 1$ take place in a thin *boundary layer* of thickness $\delta \ll L$.

Close to the wall, the velocity field is tiny because of the no-slip condition. The flow pattern will in this region always be laminar, in fact creeping, with the parallel (streamwise) velocity rising linearly from zero. The laminar flow may extend all the way to the edge of the boundary layer, or the flow may at sufficiently high Reynolds number become turbulent.

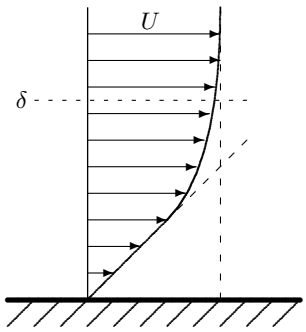

Sketch of the flow in a laminar boundary layer with constant mainstream flow. The velocity rises linearly close to the solid wall but veers off to match the mainstream flow velocity U at a characteristic distance δ from the wall. The precise layer thickness depends on a choice of what one means by "matching" the mainstream flow.

Laminar boundary layer thickness

The effective Reynolds number in a steady laminar boundary layer can be estimated from the ratio of advective to viscous terms in the Navier-Stokes equation,

$$\frac{|(\boldsymbol{v}\cdot\boldsymbol{\nabla})\boldsymbol{v}|}{|\nu\boldsymbol{\nabla}^2\boldsymbol{v}|} \sim \frac{U^2/L}{\nu U/\delta^2} = \frac{U\delta^2}{\nu L} = \frac{\delta^2}{L^2}\mathsf{Re}\ . \tag{24-1}$$

Here the numerator was estimated from the change in mainstream velocity along the wall over a distance L, using that the flow in a laminar layer must follow the geometry of the mainstream flow. The denominator was estimated from the rapid change in velocity across the thickness δ of the boundary layer.

The boundary layer is characterized by the transition from viscous dominance near the wall to advective dominance in the mainstream. We estimate the *boundary layer thickness* by requiring the effective Reynolds number (24-1) to be around unity, leading to

$$\boxed{\delta \sim \sqrt{\frac{\nu L}{U}} = \frac{L}{\sqrt{\mathsf{Re}}}}\ . \tag{24-2}$$

This estimate is valid up to a coefficient of order unity which will be discussed later (section 24.4). For large mainstream Reynolds number, $\mathsf{Re} \gg 1$, the thickness of the boundary layer will thus be considerably smaller than the typical length scale of the mainstream flow.

> The Reynolds numbers for flows we encounter in daily life easily reach into the millions, making the boundary layer thickness smaller than a thousandth of the scale of the flow. Jogging or swimming, one hardly notices the existence of boundary layers that are only millimeters thick. The pleasant tingling skin sensation you experience from streaming air or water comes presumably from the complex flow at larger scale generated by the irregular shape of your body.

Wall shear stress

In the laminar boundary layer, the velocity rises linearly with the distance from the boundary. The normal velocity gradient at the wall is approximately $\lambda \approx U/\delta$, and multiplying with the viscosity we obtain an estimate of the shear stress on the wall,

$$\sigma_{\mathsf{wall}} = \eta\lambda \approx \eta\frac{U}{\delta} \sim \frac{\rho_0 U^2}{\sqrt{\mathsf{Re}}} \ . \tag{24-3}$$

In the last expression we have also used the steady-flow estimate (24-2). The wall stress determines the *skin drag*, $\mathcal{D} = \int_A \sigma_{\mathsf{wall}}\, dS$, on a flat surface of area A. The wall stress decreases with increasing Reynolds number, in agreement with the diminishing influence of viscosity at higher Reynolds numbers.

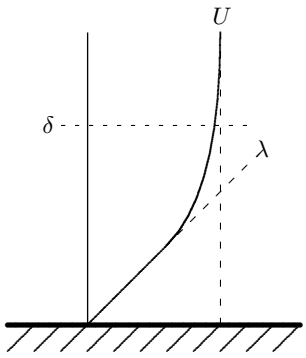

The stress on the wall of a laminar boundary layer is determined by the slope $\lambda \approx U/\delta$ of the linearly rising velocity near the wall.

Initial viscous growth

When a body in steady flow suddenly changes its velocity, the fluid immediately surrounding it will have to follow along in order to satisfy the no-slip boundary condition. Large velocity gradients and therefore large stresses will develop in the fluid next to the body, and these stresses will cause fluid layers farther out also to be dragged along. Eventually this process may come to and end and the flow will once again be steady. In the beginning the newly created boundary layer is extremely thin, so that the general geometry of the flow and the shape of the body must be unimportant. This indicates that suddenly created boundary layers always start out their growth in the same universal way.

Suppose that both body and fluid initially are at rest, and that the body at $t = 0$ is suddenly set into motion with velocity U. If the boundary layer at time $t > 0$ has reached a thickness $\delta(t)$, the fluid in the boundary layer will on the average have changed its velocity from 0 to about $\frac{1}{2}U$ in time t. This makes the local acceleration of order U/t (disregarding factors 1/2) and allows us to estimate the ratio between the local and inertial acceleration

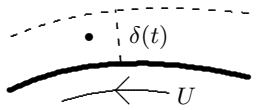

The wall is suddenly set into motion. After a time t, the velocity at a point in the middle of the growing boundary layer has changed from 0 to $\frac{1}{2}U$.

$$\frac{|\partial \boldsymbol{v}/\partial t|}{|(\boldsymbol{v}\cdot\boldsymbol{\nabla})\boldsymbol{v}|} \approx \frac{U/t}{U^2/L} = \frac{L}{Ut} \ . \tag{24-4}$$

The time the fluid takes to pass the body is L/U. For times much shorter than this, $t \ll L/U$, the inertial acceleration term can be disregarded relative to the local acceleration, and the boundary layer will continue to grow. The boundary layer cannot "go steady" until it is much older than the passing time.

In a "young" boundary layer with $t \ll L/U$, the advective acceleration can thus be disregarded, and the physics is controlled by the ratio of local to viscous acceleration,

$$\frac{|\partial \boldsymbol{v}/\partial t|}{|\nu\boldsymbol{\nabla}^2\boldsymbol{v}|} \approx \frac{U/t}{\nu U/\delta^2} = \frac{\delta^2}{\nu t} \ . \tag{24-5}$$

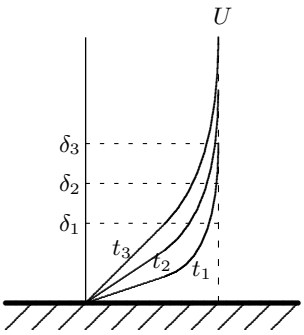

Initial growth of a laminar boundary layer. The three velocity profiles correspond to increasing times $t_1 < t_2 < t_3$ and increasing thicknesses $\delta_1 < \delta_2 < \delta_3$.

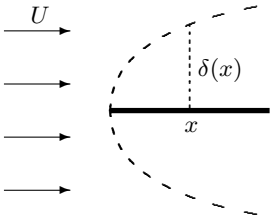

A semi-infinite plate in an otherwise uniform flow. The dashed curve is the estimated parabolic boundary layer shape.

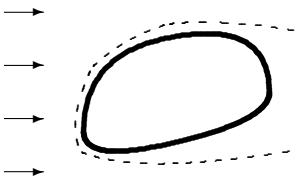

Sketch of the boundary layer around a bluff body in steady uniform flow. On the windward side the boundary layer is thin, whereas it widens and tends to separate on the lee side. In the channel formed by the separated boundary layer, unsteady flow patterns may arise.

This should be of order unity in the boundary layer, leading to

$$\boxed{\delta \sim \sqrt{\nu t} \qquad \text{for } t \ll L/U} \,. \tag{24-6}$$

A suddenly created boundary layer always starts out like this, growing with the squareroot of time. This behavior is as we have seen before typical of viscous diffusion processes, and in is of same form as the estimate of the rate of momentum diffusion (page 289) and the core expansion rate of a decaying vortex (page 361).

After the initial universal growth, the boundary layer comes to depend on the general geometry of the flow for $t \approx L/U$, when it reaches the thickness (24-2). It takes more careful analysis to see whether the flow eventually settles down into a steady boundary layer, or whether instabilities arise, leading to a radical change in the character of the flow such as boundary layer separation or turbulence.

Influence of body geometry

The simplest geometry in which a steady boundary layer can be studied is a semi-infinite plate with its edge orthogonal to a uniform mainstream flow (we shall solve this case analytically in section 24.4). Here the only possible length scale is the distance x from the leading edge, so that we must have

$$\delta \sim \sqrt{\frac{\nu x}{U}} \,. \tag{24-7}$$

This shows that boundary layers tend to grow thicker downstream, even if the mainstream flow is completely uniform and independent of x. If the flat plate is set abruptly into motion, the initial growth of the layer at a downstream distance x steadies at time $t \approx x/U$. Disregarding sound waves, the time $t = x/U$ is also the earliest moment that the edge causally can influence the flow near x. Intuitively one might say that the viscous growth of the boundary layer is curtailed by the encounter with the blast of undisturbed fluid coming in from afar.

Boundary layers have a natural tendency towards *downstream thickening*, because they build up along a body in a cumulative fashion. Having reached a certain thickness, a boundary layer acts as a not-quite-solid "wall" on which another boundary layer will form. The thickness of a steady boundary layer is also strongly dependent on whether the mainstream flow is accelerating or decelerating along the body, behavior which in turn is determined by the geometry. If the mainstream flow accelerates, *i.e.* grows with x, the boundary layer tends to remain thin. This happens at the front of a moving body, where the fluid must speed up to get out of the way. Conversely, towards the rear of the body, where the mainstream flow again decelerates in order to "fill up the hole" left by the passing body, the boundary layer becomes rapidly thicker, and may even separate from the body, creating an unsteady, often turbulent, *trailing wake*.

Merging boundary layers

The increase of a boundary layer's thickness with body size implies for an infinite body that the boundary layer must be infinitely thick or at least so thick that it fills out all the available space. In steady planar flow between moving plates (section 17.1), the velocity profile of the fluid interpolates linearly between the plate velocities, and one sees nothing like a boundary layer with finite thickness near the plates. In pressure-driven steady pipe flow (section 18.6), the exact shape of the Poiseuille velocity profile is parabolic (as long as the flow is laminar), whatever the viscosity of the fluid. Again we see no trace of a finite boundary layer in the exact solution.

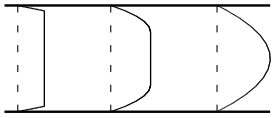

Sketch of the shape of the velocity profile in pressure-driven flow between half-infinite plates at various distances downstream from the entrance at the left.

Consider now pressure-driven flow between two half-infinite plates, a distance d apart. The boundary layers grow like $\sqrt{x}$ from both sides downstream from the entrance and eventually merge with each other at a typical distance $x = L'$, called the *entrance length*. Further downstream, the Poiseuille profile is established, and the distinction between boundary and mainstream flow is no more possible. The two boundary layers meet at $x = L'$, determined by solving the equation $2\delta(x) \approx d$. Using a conservative estimate $\delta(x) \approx 3\sqrt{\nu x/U}$, the entrance length becomes

$$L' \approx \frac{d}{36}\,\mathsf{Re} \tag{24-8}$$

with $\mathsf{Re} = Ud/\nu \gg 1$. The numerical computation in section 19.4 showed that this estimate is in fact not far off the mark.

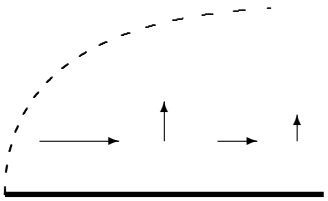

The thickening of a boundary layer decelerates the flow and leads to upwelling of fluid from the boundary.

Upwelling and downwash

Inside a boundary layer, at a fixed distance from a flat solid wall with a uniform mainstream velocity U, the flow decelerates downstream as the boundary layer thickens due to the action of viscosity. Mass conservation requires a compensating *upwelling* of fluid into the fluid at large. If the boundary is permeable and fluid is sucked down through it at a constant rate, the upflow can be avoided, and a steady boundary layer of constant thickness may be created (problem 24.1).

The mainstream flow is determined by bodies and containers that guide the fluid and will generally not be uniform but rather accelerate or decelerate along the boundaries. An accelerating mainstream flow will counteract the natural deceleration in the boundary layer and may even overwhelm it, leading to a *downwash* towards the boundary. Mainstream acceleration thus tends to stabilize a boundary layer so that it has less tendency to thicken, and may lead to constant or even diminishing thickness. Conversely, if the mainstream flow decelerates, this will add to the natural deceleration in the boundary layer and increase its thickness as well as the upwelling.

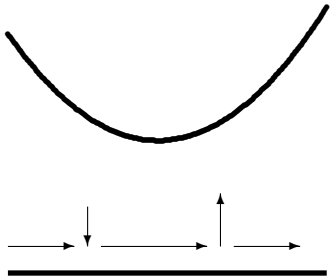

Mainstream acceleration in a converging channel produces a downwash of fluid, and conversely in a diverging channel.

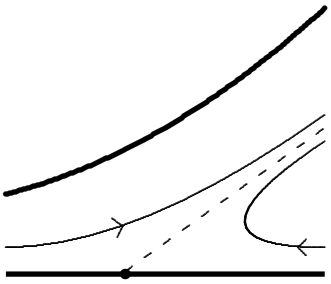

Flow reversal and boundary layer separation in a diverging channel with decelerating flow.

Separation

Even at very moderate mainstream deceleration, the upwelling can become so strong at some point that the fluid flowing in the mainstream direction cannot feed it. Some of the fluid in the boundary layer will then have to flow against the mainstream flow. Between the forward and reversed flows there will be a separation line ending on the wall. Such *flow reversal* was also noticed in lubrication (page 397), although there are no boundary layers in creeping flow.

In the region of reversed flow, the velocity still has to vanish right at the boundary. Moving up from the boundary wall, the flow first moves backwards with respect to the mainstream, but farther from the wall it must again turn back to join up with the mainstream. The velocity gradient must accordingly be negative right at the boundary in the reversal region, corresponding to a negative wall stress σ_{wall}. The vanishing of the wall stress, $\sigma_{\mathsf{wall}} = 0$, indicates that boundary layer separation may happen. It is not a sufficient condition, because flow reversal can in principle be a local phenomenon taking place entirely within the boundary layer, as may be the case if there is a dent in the wall.

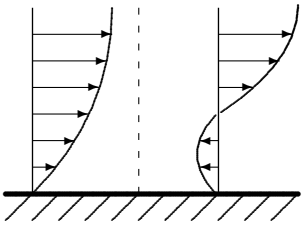

Velocity profiles before and after the separation point (dashed line).

Turbulence

Boundary layers can also become turbulent. Turbulence efficiently mixes fluid in all directions. The orderly layers of fluid that otherwise isolate the wall from the mainstream flow all but disappear, and on average, the mainstream velocity will press much closer to the wall. Turbulence typically sets in downstream from the front of body when the laminar boundary layer has grown so thick that the *local Reynolds number*

$$\mathsf{Re}_\delta = \frac{U\delta}{\nu} \ , \tag{24-9}$$

becomes large enough, say in the thousands.. In a laminar boundary layer, the estimate (24-2) shows that $\mathsf{Re} \sim \mathsf{Re}_\delta^2$, so that turbulence will not arise until the mainstream Reynolds number reaches into the millions, which incidentally is just about the range in which humans and many of their machines operate.

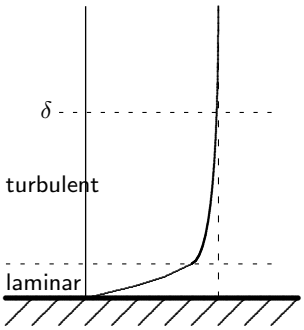

In a turbulent boundary layer there will always be a thin nearly laminar sublayer, in which the velocity profile rises linearly from the wall.

Although the turbulent velocity fluctuations press close to the wall, there will always remain a thin viscous, nearly laminar, sublayer close to the wall, in which the average velocity gradient normal to the wall rises linearly with distance. Since the mainstream velocity on average comes much closer to the wall, the average wall stress will be much larger than in a completely laminar boundary layer. The skin drag on a body is consequently expected to increase when the boundary layer becomes turbulent, though other changes in the flow may interfere and instead cause an even larger drop in the form drag at a particular value of the Reynolds number, as we saw in the discussion of the "drag crisis" (page 385).

The phenomenology of turbulent boundary layers is discussed in some detail for a flat plate in section 24.5.

24.2 Growth of a boundary layer

The initial growth of the boundary layer near a flat plate which is suddenly set into motion (Stokes first problem) must also follow the universal law (24-6). In this case there is no intrinsic length scale for the geometry, and the transition to geometry-dependent steady flow cannot take place. The planar boundary layer (called the Stokes layer) can for this reason be expected to provide a clean model for universal viscous growth.

Analytic solution

As usual it is more convenient to view the plate from the reference frame in which the plate and the fluid initially move with the same velocity U and the plate is suddenly stopped at $t = 0$. Assuming that the flow is planar with $v_x = v_x(y,t)$ and $v_y = 0$, the Navier-Stokes equation for incompressible flow reduces to the momentum-diffusion equation (17-7), which is repeated here for convenience

$$\frac{\partial v_x}{\partial t} = \nu \frac{\partial^2 v_x}{\partial y^2} \ . \tag{24-10}$$

The linearity of this equation guarantees that the velocity everywhere must be proportional to U, and since there is no intrinsic length or time scale in the definition of the problem, the velocity field must be of the form,

$$v_x(y,t) = U f(s) \ , \qquad s = \frac{y}{\sqrt{2\nu t}} \tag{24-11}$$

where the so far unknown function $f(s)$ should obey the boundary conditions $f(0) = 0$ and $f(\infty) = 1$. The factor 2 in the squareroot is conventional.

Upon insertion of (24-11) into (24-10) we are lead to an ordinary second order differential equation for $f(s)$,

$$\boxed{f''(s) + s f'(s) = 0} \ . \tag{24-12}$$

Viewed as a first order equation for $f'(s)$, it has the unique solution $f'(s) \sim \exp(-s^2/2)$. Integrating this expression once more over s and applying the boundary conditions, the final result becomes

$$f(s) = \sqrt{\frac{2}{\pi}} \int_0^s e^{-s'^2/2} \, ds' = \mathrm{erf}\left(\frac{s}{\sqrt{2}}\right) \ , \tag{24-13}$$

where $\mathrm{erf}(\cdot)$ is the well-known error function. For small values of s we have $f(s) \approx s\sqrt{2/\pi}$ whereas for large values the function approaches 1 with a Gaussian tail, $1 - f(s) \sim \exp(-s^2/2) = \exp(-y^2/4\nu t)$, typical of momentum diffusion (see page 289).

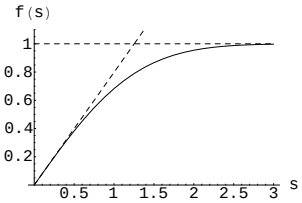

Plot of $f(s)$. The sloping dashed line is tangent at $s = 0$ with inclination $f'(0) = \sqrt{2/\pi}$.

The Gaussian tail

Notice that the Gaussian tail of the boundary layer extends all the way to spatial infinity for *any* positive time, $t > 0$. How can that be, when the plate was only brought to stop at time $t = 0$? Won't it take a finite time for this event to propagate to spatial infinity? The short answer is that we have assumed the fluid to be incompressible, and this — fundamentally untenable — assumption will in itself entail infinite signal speeds. At a deeper level, a diffusion equation like (24-10) is the statistical continuum limit of the dynamics of random molecular motion in the fluid, and although extremely high molecular speeds are strongly damped, they may in principle occur. The limit to diffusion speed as well as to incompressibility is, as discussed before, always set by the finite speed of sound.

Vorticity generation

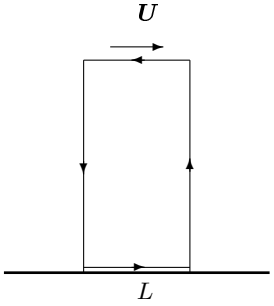

The circulation around an infinitely tall rectangle with side L against the moving wall is $\oint \boldsymbol{v} \cdot d\boldsymbol{\ell} = -UL$.

The vorticity field has only one component

$$\omega_z(y,t) = -\frac{\partial v_x(y,t)}{\partial y} = -\frac{U f'(s)}{\sqrt{2\nu t}} = -\frac{U}{\sqrt{\pi\nu t}} e^{-y^2/4\nu t} \tag{24-14}$$

Before the plate stopped, the flow was everywhere irrotational. Afterwards there is evidently vorticity in the boundary layer. Where did it come from?

Consider a (nearly) infinite rectangle with support of length L on the plate. The flow in the boundary layer has a total flux of vorticity (or circulation) $\Gamma = \int \boldsymbol{\omega} \cdot d\boldsymbol{S} = \oint \boldsymbol{v} \cdot d\boldsymbol{\ell}$ through this rectangle. The fluid velocity always vanishes on the plate, is orthogonal to the sides, and approaches the constant U at infinity, so that we obtain $\Gamma = -UL$. Since the circulation is constant in time, vorticity is not generated inside the boundary layer itself during its growth, but rather at the plate surface during the instantaneous deceleration to zero velocity. If the plate did not stop with infinite deceleration, but followed a gentler path $U(t)$ from U to 0, the circulation $\Gamma(t) = (U(t) - U)L$ would also have decreased gently from 0 to $-UL$. The conclusion is that vorticity is originally generated at the plate surface during acceleration and deceleration. Afterwards it diffuses away from the plate and into the fluid at large without changing the total circulation.

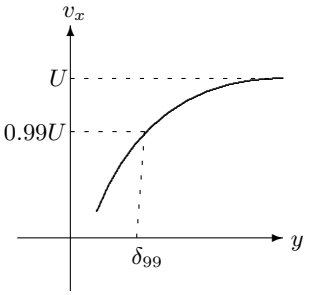

Definition of conventional thickness δ_{99} as the distance from the wall where the velocity has reached 99% of the mainstream velocity U.

Thickness

The velocity field is self-similar in the sense that it has similarly shaped velocity profile $f(y/\sqrt{2\nu t})$ at all times. There is no cut-off in the infinitely extended Gaussian tail and therefore no "true" thickness δ. Conventionally, one defines the boundary layer thickness to be where the velocity has reached 99% of terminal velocity. The solution to $f(k) = 0.99$ is $k = 2.5783\ldots$, so that

$$\delta_{99} = k\sqrt{2\nu t} \approx 3.64\sqrt{\nu t}\ . \tag{24-15}$$

In the following section we shall meet other and less arbitrary definitions of boundary layer thickness.

24.3 Boundary layer theory

In his short 1904 paper [14] Prandtl introduced the concept of boundary layers and pointed out that there were simplifying features, allowing for less complicated equations than the full set of Navier and Stokes. The greater simplicity comes from the assumption of nearly ideal mainstream flow with $\mathsf{Re} \gg 1$, which according to the estimate (24-2) implies that boundary layers are thin, *i.e.* $\delta \ll L$ where L is the length scale for variations in the mainstream flow.

We shall — as Prandtl did — consider only the two-dimensional case with an infinitely extended planar boundary wall at $y = 0$ and a unidirectional mainstream flow along x. The analysis can be extended to a curved boundary, as long as the boundary layer is much thinner than the radius of curvature R of the wall, $\delta \ll R$. In that case, the coordinates should be understood as curvilinear with the x-coordinate following the shape of the wall and the y-coordinate always pointing along the local normal.

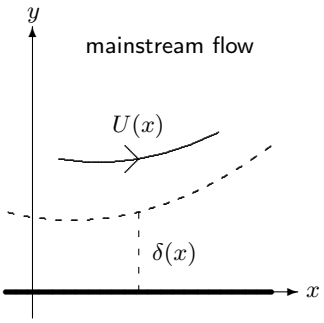

Geometry of two-dimensional planar boundary flow. In the absence of viscosity there would be a slowly varying ideal slip-flow $U(x)$ along the boundary. Viscosity interposes a thin boundary layer of thickness $\delta(x)$ between the slip-flow and the boundary.

Ideal slip-flow

In the absence of viscosity, the incompressible ideal fluid would slip along the boundary, $y = 0$, with a slowly varying *slip-velocity*, $v_x = U(x)$. Leaving out gravity, it follows from Bernoulli's theorem (15-12) that there must be an associated slip-flow pressure at the boundary,

$$P(x) = P_0 - \frac{1}{2}\rho_0 U(x)^2 \ , \tag{24-16}$$

where P_0 is a constant. The slip-flow pressure simply reflects the variation in slip-velocity along the boundary. Even in the ideal case there will also be an upflow close to the boundary implied by mass conservation, *i.e.* the continuity equation

$$\frac{\partial v_x}{\partial x} + \frac{\partial v_y}{\partial y} = 0 \ . \tag{24-17}$$

Inserting $v_x = U(x)$ and using that $v_y = 0$ for $y = 0$, we have

$$v_y = -y\frac{dU(x)}{dx} \tag{24-18}$$

Only for constant $U(x) = U_0$ will this upflow from the boundary layer be absent. It is generally negligible compared to U inside the boundary layer, $y \lesssim \delta$.

The no-slip condition implies that the true velocity must change rapidly from $v_x = 0$ right at the boundary, $y = 0$, to $v_x = U(x)$ outside the boundary layer. Formulated more carefully, the slip-flow velocity $U(x)$ and boundary pressure $P(x)$ should be understood as describing the flow in the region $\delta \ll y \ll L$, well outside the boundary layer but still so close to the boundary that the mainstream flow only depends on x. In the mainstream proper for $y \gtrsim L$, flow and pressure depend on both x and y with a typical length scale L for major variations. So even if the upflow appears to grow indefinitely, it will be become part of the mainstream flow for $y \gtrsim L$.

The Prandtl equations

In the boundary layer v_x depends also on y. Integrating the equation of continuity over y, and using the boundary condition $v_y = 0$ for $y = 0$, we obtain the general exact relation,

$$\boxed{v_y(x,y) = -\frac{\partial}{\partial x}\int_0^y v_x(x,y')\,dy'} \ . \tag{24-19}$$

Inside the boundary layer for $y \lesssim \delta$, this equation permits us to estimate $v_y \approx U\,\delta/L \sim U/\sqrt{\mathsf{Re}}$. The upflow from the boundary layer will thus in general for $\mathsf{Re} \gg 1$ be much smaller than the slipflow.

In two dimensions the steady-flow Navier-Stokes equations (18-2) take the form

$$v_x\frac{\partial v_x}{\partial x} + v_y\frac{\partial v_x}{\partial y} = -\frac{1}{\rho_0}\frac{\partial p}{\partial x} + \nu\left(\frac{\partial^2 v_x}{\partial x^2} + \frac{\partial^2 v_x}{\partial y^2}\right) \ , \tag{24-20a}$$

$$v_x\frac{\partial v_y}{\partial x} + v_y\frac{\partial v_y}{\partial y} = -\frac{1}{\rho_0}\frac{\partial p}{\partial y} + \nu\left(\frac{\partial^2 v_y}{\partial x^2} + \frac{\partial^2 v_y}{\partial y^2}\right) \ . \tag{24-20b}$$

In either of these equations, the double derivative after y is proportional to $1/\delta^2$, whereas the double derivative after x is proportional to $1/L^2$, making it a factor $1/\mathsf{Re}$ smaller and thus negligible for $\mathsf{Re} \to \infty$. From the estimate of the thickness of the boundary layer (24-2) it follows that the viscous terms on the right are of the same order of magnitude as the advective terms on the left, which are also both of comparable magnitude. Setting $v_x \approx U$ and $v_y \approx U\delta/L$ we estimate from any of the remaining terms in the second equation that the normal pressure gradient is $\partial p/\partial y \approx \rho_0 U^2\delta/L^2$. Finally, multiplying this expression with δ we obtain the pressure variation across the boundary layer $\Delta_y p \approx \delta\,\partial p/\partial y \approx \rho_0 U^2\delta^2/L^2 \sim \rho_0 U^2/\mathsf{Re}$. This is much smaller, by roughly a factor $1/\mathsf{Re}$, than the typical variation in slip-flow pressure (24-16), $\Delta p \approx \rho_0 U^2$ and may thus be disregarded in this approximation. The true pressure in the boundary layer is accordingly essentially equal to the slip-flow pressure, $p(x,y) \approx P(x)$.

Inserting $p = P$ in (24-20a) and dropping the second order derivative after x, we arrive at *Prandtl's momentum equation*,

$$\boxed{v_x\frac{\partial v_x}{\partial x} + v_y\frac{\partial v_x}{\partial y} = U\frac{dU}{dx} + \nu\frac{\partial^2 v_x}{\partial y^2}} \ . \tag{24-21}$$

Since v_y is given in terms of v_x by (24-19), we have obtained a single integro-differential equation which for any given $U(x)$ determines v_x, subject to the boundary conditions $v_x = 0$ for $y = 0$ and $v_x \to U$ for $y \to \infty$. The preceding analysis shows that the correction terms to this equation are of order $1/\mathsf{Re}$. The Prandtl approximation breaks down near a separation point, where the upflow becomes comparable to the mainflow.

24.4 Laminar boundary layer in uniform flow

The generic example of a steady laminar boundary layer is furnished by a semi-infinite plate with its edge orthogonal to a uniform flow with constant velocity U, a problem first solved by Blasius in 1908.

Paul Richard Heinrich Blasius (1883–1970). *German physicist, a student of Prandtl. Worked on boundary-layer drag and smooth pipe resistance.*

Self-similarity

As the main variation in v_x happens across the boundary layer, it may be convenient to measure y in units of the thickness of the boundary layer, estimated to be of order $\delta \sim \sqrt{\nu x/U}$ on page 410. Let us for this reason write the velocity in dimensionless self-similar form,

$$v_x(x,y) = U f(s) \ , \qquad s = y\sqrt{\frac{U}{2\nu x}} \ , \tag{24-22}$$

where $f(s)$ must satisfy the boundary conditions, $f(0) = 0$ and $f(\infty) = 1$. The factor of 2 in the squareroot is conventional. In principle the function could also depend on the dimensionless variable $\mathsf{Re}_x = Ux/\nu$, but the correctness of the above assumption will be justified by finding a solution satisfying the boundary conditions.

Upflow

From the equation of continuity (24-19) we obtain

$$v_y(x,y) = -\frac{\partial}{\partial x}\int_0^y v_x(x,y')\,dy' = -\frac{\partial}{\partial x}\left[\sqrt{2U\nu x}\ g(s)\right] \ .$$

Here we have for convenience defined the integral

$$g(s) = \int_0^s f(s')\,ds' \tag{24-23}$$

so that $f(s) = g'(s)$. Carrying out the differentiation, we obtain the upflow from the layer,

$$v_y(x,y) = h(s)\sqrt{\frac{U\nu}{2x}} \ , \tag{24-24}$$

with

$$h(s) = sf(s) - g(s) \ . \tag{24-25}$$

The asymptotic value $h(\infty) = \lim_{s\to\infty}(s - g(s))$ determines the total upflow from the boundary layer into the mainstream.

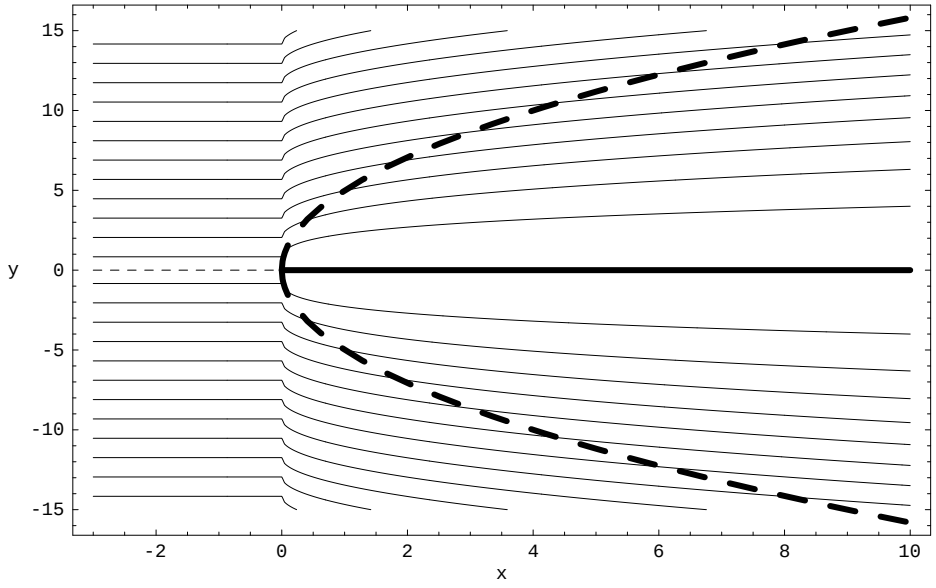

Figure 24.1: *Streamlines around a semi-infinite thin plate with fluid flowing uniformly in from the left (see problem 24.5). Units are chosen so that $U = \nu = 1$. The thin dashed streamline terminates in a stagnation point. The heavy dashed curve indicates the 99% thickness, $y = \delta = 5\sqrt{x}$. The kink in the streamlines at $x = 0$ signals breakdown of the Prandtl approximation in this region.*

Blasius' equation

Finally, v_y is inserted into the Prandtl equation (24-21) and using that in this case U is constant, we obtain a single third order ordinary differential equation, called *Blasius' equation*,

$$\boxed{g'''(s) + g(s)g''(s) = 0}\,, \tag{24-26}$$

which must be solved with the boundary conditions $g(0) = 0$, $g'(0) = f(0) = 0$, and $g'(\infty) = f(\infty) = 1$. Numeric integration yields the results shown in fig. 24.1 and 24.2.

The condition $g'(\infty) = 1$ seems at first a bit troublesome to implement. The trick is first to find the solution $\widetilde{g}(s)$ which satisfies the Blasius equation with with $\widetilde{g}''(0) = 1$. This solution converges at infinity to a value $\alpha = \widetilde{g}'(\infty) = 1.65519\ldots$ instead of unity. The correct solution is finally obtained by the transformation,

$$g(s) = \frac{1}{\sqrt{\alpha}}\widetilde{g}\left(\frac{s}{\sqrt{\alpha}}\right) \tag{24-27}$$

It is a simple matter to verify that this function also satisfies the Blasius equation.

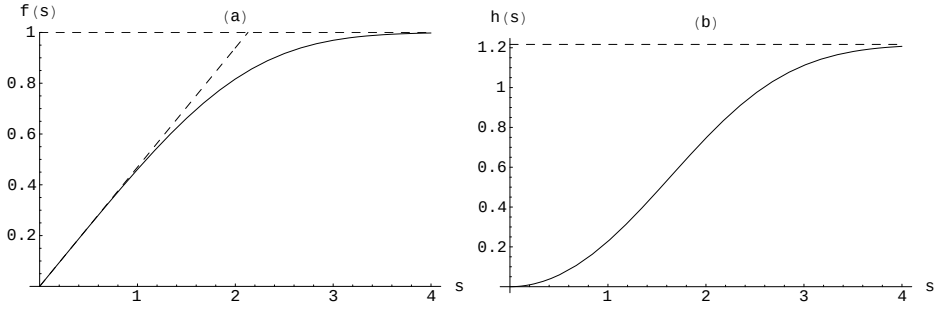

Figure 24.2: *Plot of the self-similar shape functions for (a) $v_x = Uf(s)$, and (b) $v_y = h(s)\sqrt{U\nu/2x}$. The dashed line in pane (a) has slope $f'(0) = 0.46960\ldots$ and is tangent at $s = 0$. It crosses unity at $s = 2.1295$. The dashed line in pane (b) indicates the asymptotic value $h(\infty) = 1.21678\ldots$ and determines the resulting upwelling of fluid from the boundary layer into the mainstream flow.*

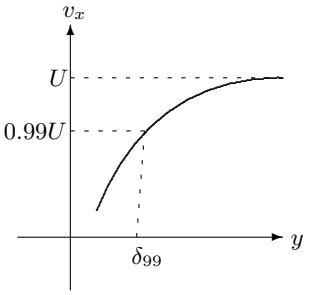

Definition of conventional thickness δ_{99} as the distance from the wall where the velocity has reached 99% of the mainstream velocity U.

Thickness and local Reynolds number

The conventional thickness of the Blasius layer is as for the Stokes layer (section 24.2) defined to be the distance $y = \delta$ where the velocity has reached 99% of the slip-flow velocity, which happens for $f(s) = 0.99$. The solution of this equation is $s = 3.4719\ldots$, so that the thickness becomes

$$\delta_{99} = 3.4719\ldots\sqrt{\frac{2\nu x}{U}} \approx 4.91\sqrt{\frac{\nu x}{U}}\ . \tag{24-28}$$

Typically, one uses $\delta \approx 5\sqrt{\nu x/U}$ for estimates. In dimensionless form, this may be expressed in terms of the local Reynolds number,

$$\mathsf{Re}_\delta = \frac{U\delta}{\nu} \approx 5\sqrt{\mathsf{Re}_x}\ , \tag{24-29}$$

where as before $\mathsf{Re}_x = Ux/\nu$ is the "downstream" Reynolds number. Turbulence typically sets in for a local Reynolds number between 2000 and 4000.

Wall stress and friction coefficient

The wall stress becomes

$$\sigma_{\mathsf{wall}} = \eta\left.\frac{\partial v_x}{\partial y}\right|_{y=0} = \eta U\sqrt{\frac{U}{2\nu x}}f'(0) \tag{24-30}$$

It is customary also to make the wall stress dimensionless by dividing with $\frac{1}{2}\rho_0 U^2$ to get the so-called *local friction coefficient*,

$$c_f \equiv \frac{\sigma_{\mathsf{wall}}}{\frac{1}{2}\rho_0 U^2} = f'(0)\sqrt{\frac{2}{\mathsf{Re}_x}} \approx \frac{0.664}{\sqrt{\mathsf{Re}_x}}\ , \tag{24-31}$$

In a turbulent boundary layer (section 24.5), this expression is replaced by a semi-empirical power law of the same general form but with a different power and coefficient. Notice the singularity at $x = 0$, which signals breakdown of the boundary layer approximation at the leading edge of the plate.

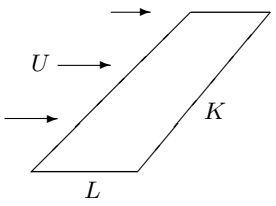

A flat and thin wing aligned with the flow only experiences skin drag.

Laminar skin drag on a flat wing

Consider now an infinitely thin rectangular "wing" with "chord" L in the direction of flow, and a "span" K orthogonal to the flow (in the z-direction). Such an object generates no form drag, when it is aligned with the flow. Disregarding the influence of the rear and side edges of the wing, the total (skin) drag is obtained by integrating $\sigma_{\mathsf{wall}} = \frac{1}{2}\rho_0 U^2 c_f$ over both sides of the plate,

$$\mathcal{D} = 2\int_0^L \sigma_{\mathsf{wall}}(x)\, K dx = 2\eta U K f'(0) \int_0^L \sqrt{\frac{U}{2\nu x}}\, dx = 4\eta U K f'(0)\sqrt{\frac{UL}{2\nu}}\ .$$

This becomes more transparent when expressed in terms of the dimensionless *drag coefficient* for the wing,

$$C_{\mathcal{D}} = \frac{\mathcal{D}}{\frac{1}{2}\rho_0 U^2 A} = \frac{8f'(0)}{\sqrt{2\mathsf{Re}}} \approx \frac{2.6565}{\sqrt{\mathsf{Re}}}, \tag{24-32}$$

where $A = KL$ is the wing's area and $\mathsf{Re} = UL/\nu$ is its wing's Reynolds number. The skin drag coefficient decreases with the squareroot of the Reynolds number, and is of little importance in most everyday situations with Reynolds number in the millions. The skin drag is mostly dominated by the form drag coefficient which does not decrease but rather stays constant for $\mathsf{Re} \to \infty$.

Example 24.4.1 (Weather vane): A little rectangular metal weather vane with sides $L = 30$ cm and $K = 20$ cm in a 10 m s^{-1} wind has $\mathsf{Re} = UL/\nu \approx 200,000$, well below the onset of turbulence. The drag coefficient becomes $C_{\mathcal{D}} \approx 0.0059$ and the total skin drag $\mathcal{D} \approx 0.018$ N, when the vane aligned with the wind. This drag corresponds to a weight of merely 2 g, whereas the form drag and the other aerodynamic forces that align the vane are much stronger. One should not dimension the support of the vane on the basis of the laminar skin drag!

24.5 Turbulent boundary layer in uniform flow

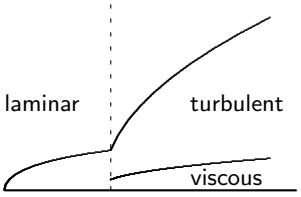

Sketch of the shape of the boundary layer from the leading edge through the transition region. At the transition (dashed line), the turbulent layer grows rapidly whereas the viscous sublayer only grows slowly.

Sufficiently far downstream from the leading edge, the Reynolds number, $\mathsf{Re}_x = Ux/\nu$, will eventually grow so large that the boundary layer becomes turbulent. Empirically, the transition happens for $5 \times 10^5 \lesssim \mathsf{Re}_x \lesssim 3 \times 10^6$, depending on the circumstances, for example the uniformity of the mainstream flow and the roughness of the plate surface. We shall in the following discussion take $\mathcal{R}e_x = 5 \times 10^5$ as the nominal transition point.

The line of transition across the plate is not a straight line parallel with the z-axis, but rather an irregular, time-dependent, jagged, even fractal interface between the laminar and turbulent regions. This is also the case for the extended, nearly "horizontal" interface between the turbulent boundary layer and the fluid at large. Such intermittent and fractal behavior is common to the onset of turbulence in all systems.

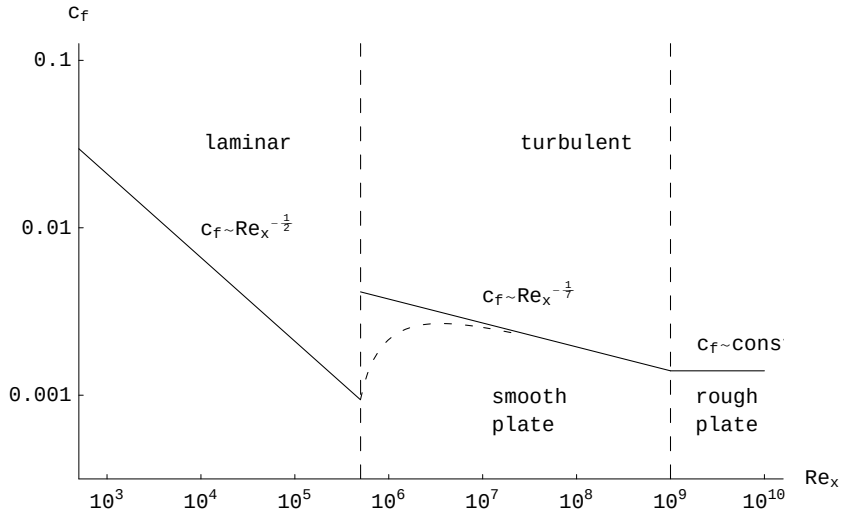

Figure 24.3: *Schematic plot of the local friction coefficient* $c_f = 2\bar{\sigma}_{wall}(x)/\rho_0 U^2$ *across the laminar and turbulent regions as a function of the downstream Reynolds number* $\mathsf{Re}_x = Ux/\nu$. *The transitions at the nominal points* $\mathsf{Re}_x = 5 \times 10^5$ *and* 10^9 *are in reality considerably softer than shown here (with the dashed curve as a possible transition shape). The position of the second transition and the terminal value of* c_f *depend on the roughness of the plate surface (see [36] for details).*

Friction coefficient

In a turbulent boundary layer, the true velocity field $\boldsymbol{v}$ fluctuates in all directions and in time around some mean value. Even very close to the wall, there will be noticeable fluctuations. The no-slip condition nevertheless has to be fulfilled and a thin sublayer dominated by viscous stresses must exist close to the wall. In this viscous sublayer the average velocity $\bar{v}_x$ rises linearly from the surface with a slope, $\partial\bar{v}_x/\partial y|_{y=0} = \bar{\sigma}_{\mathsf{wall}}/\eta$ that can be determined from drag measurements.

A decent semi-empirical expression for the friction coefficient of a turbulent boundary layer is

$$c_f \equiv \frac{\bar{\sigma}_{\mathsf{wall}}}{\frac{1}{2}\rho_0 U^2} \approx \frac{0.027}{\mathsf{Re}_x^{1/7}} \ . \tag{24-33}$$

The turbulent friction coefficient thus decreases much slower than the corresponding laminar friction coefficient (24-31). The two expressions cross each other at $\mathsf{Re}_x \approx 7800$ which is far below the transition to turbulence , implying a jump from $c_f \approx 9.4 \times 10^{-4}$ to $c_f \approx 4.1 \times 10^{-3}$ at $\mathsf{Re}_x \approx 5 \times 10^5$. Turbulent boundary layers thus cause much more skin drag than laminar boundary layers (by a factor of more than 4 at the nominal transition point).

In fig. 24.3 the friction coefficient is plotted across the laminar and turbulent regimes. The transition from laminar to turbulent is in reality not nearly as sharp as shown here, partly because of the average over the jagged transition line. Eventually, for sufficiently large Re_x, the roughness of the plate surface makes the friction coefficient nearly independent of viscosity and thus of Re_x.

Drag on a flat wing

Let us again consider a finite "wing" of size $A = L \times K$. For sufficiently large Reynolds number $\mathsf{Re} = UL/\nu$, the boundary layer will always become turbulent some distance downstream from the the leading edge, and the skin drag will in general be dominated by the turbulent boundary layer's larger friction coefficient. For a fully turbulent boundary layer, the dimensionless turbulent drag coefficient becomes (including both sides of the plate)

$$C_{\mathcal{D}} = \frac{2}{\frac{1}{2}\rho_0 U^2 A} \int_0^L \bar{\sigma}_{\mathsf{wall}}(x)\, K dx = \frac{0.063}{\mathsf{Re}^{1/7}} \tag{24-34}$$

where $A = KL$ as before is the wing area. If the leading laminar boundary layer cannot be disregarded, this expression is somewhat modified.

Example 24.5.1: A 2×2 m^2 flag in a 10 $\mathsf{m\ s}^{-1}$ wind has a Reynolds number of $\mathsf{Re} \approx 1.3 \times 10^6$, well inside the turbulent region. The laminar skin drag coefficient is $C_{\mathcal{D}} \approx 0.0023$ whereas the turbulent skin drag coefficient is $C_{\mathcal{D}} \approx 0.0084$. The turbulent skin drag is only $\mathcal{D} \approx 1.68$ N which seems much too small to keep the flag straight. But flags tend to flap irregularly in the wind, thereby adding a much larger average form drag to the total drag, and giving it even in a moderate wind the nearly straight form that we admire so much. The straight flag in the wind is an image so ingrained in our minds that NASA chose to simulate it when planting an aluminium edition of Stars and Stripes in the soil of the airless Moon.

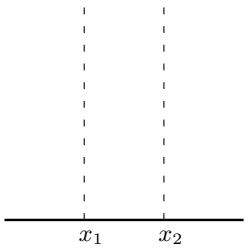

The drag on the plate between x_1 and x_2 must equal the rate of loss of momentum from the fluid between the dashed lines.

Local drag and momentum balance

Momentum balance guarantees that the drag on any section of the plate, say for $x_1 < x < x_2$, must equal the rate of momentum loss from the slice of fluid above this interval, independently of whether the fluid is laminar or turbulent. Formally, we may use the Prandtl equations to derive such a relation for an infinitesimal slice of the boundary layer, as was first done by von Kármán in 1921.

Theodore von Kármán (1881-1963). *Influential Hungarian-American engineer. Lived from 1930 in the US, and became in 1944 cofounder of the Jet Propulsion Laboratory at the California Institute of Technology. Made major contributions to the understanding of fluid mechanics, aircraft structures, rocket propulsion, and soil erosion. A crater on the Moon bears his name today.*

For constant slip-flow it follows trivially from (24-19) and (24-21) that

$$-\nu \frac{\partial^2 v_x}{\partial y^2} = \frac{\partial((U - v_x)v_x)}{\partial x} + \frac{\partial(v_y(U - v_x))}{\partial y} \ . \tag{24-35}$$

Integrating over all y and using the boundary conditions, we see that the second term on the right hand side does not contribute, and we obtain

$$\nu \left.\frac{\partial v_x}{\partial y}\right|_{y=0} = \frac{d}{dx} \int_0^\infty (U - v_x)v_x \, dy \ . \tag{24-36}$$

The quantity on the left hand side is simply $\sigma_{\mathsf{wall}}/\rho_0$, and the integral on the right hand side is the flux of lost momentum. In section 24.6 we shall make a more systematic study of such relations.

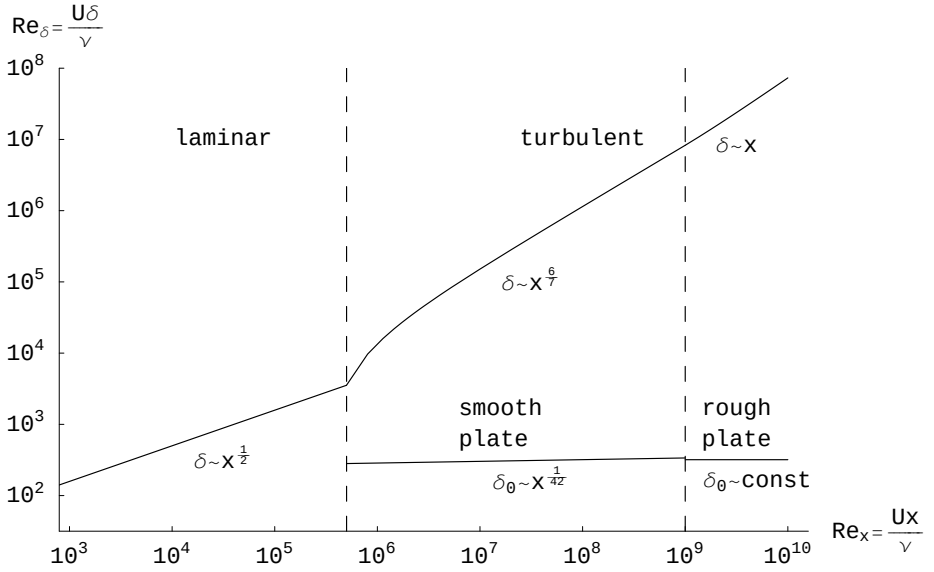

Figure 24.4: *Schematic plot of the dimensionless "true" thickness, represented by* $\mathsf{Re}_\delta = U\delta/\nu$*, as a function of downstream distance* x*, represented by* $\mathsf{Re}_x = Ux/\nu$*. Also shown is the thickness of the viscous sublayer* δ_0*. The momentum thickness* δ_{mom} *is obtained from the refined expression (24-42) and is everywhere roughly a factor 10 smaller than the "true" thickness* δ*. The real transition at the nominal value,* $\mathsf{Re}_x = 5 \times 10^5$*, is even softer than shown here. The transition from smooth to rough plate at* $\mathsf{Re} = 10^9$ *is barely visible.*

Turbulent velocity profile and thickness

Empirically, the flat-plate turbulent boundary layer profile outside the viscous sublayer is decently described by the simple model (due to Prandtl),

$$\frac{v_x}{U} = \left(\frac{y}{\delta}\right)^{1/7} , \qquad (0 \lesssim y < \delta) . \tag{24-37}$$

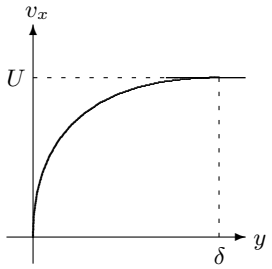

The turbulent velocity profile is approximately a power $\bar{v}_x \sim y^\gamma$ *with* $\gamma \approx 1/7$*. The vertical tangent at* $y = 0$ *is unphysical, because it implies infinite wall stress.*

Although the thickness δ is not known at this stage, we may use the von Kármán relation (24-36) to relate it to the friction coefficient, for which we have the semi-empirical expression (24-33). Ignoring the thin viscous sublayer which cannot contribute much to the integral, we obtain

$$\int_0^\delta (U - v_x) v_x \, dy = \frac{7}{72} U^2 \delta . \tag{24-38}$$

The von Kármán relation now becomes a differential equation for the thickness,

$$\frac{d\delta}{dx} = \frac{36}{7} c_f . \tag{24-39}$$

In a fully turbulent boundary layer, we may integrate this equation using (24-33) with the initial value $\delta = 0$ at $x = 0$, to get

$$\delta = \frac{36}{7} \int_0^x c_f \, dx \approx 0.16 \frac{\nu}{U} \mathsf{Re}_x^{6/7} . \tag{24-40}$$

Expressing the thickness in dimensionless form by means of the local Reynolds number, we finally have

$$\boxed{\mathsf{Re}_\delta \equiv \frac{U\delta}{\nu} = 0.16\,\mathsf{Re}_x^{6/7}} \ . \tag{24-41}$$

The jump in the local Reynolds number at the nominal transition point $x = x_0$ where $\mathsf{Re}_{x_0} = 5 \times 10^5$, is only apparent. A more precise expression for the local Reynolds number may be obtained by using the Blasius result for $0 \le x \le x_0$, and integrating the turbulent expression only for $x > x_0$,

$$\mathsf{Re}_\delta = \begin{cases} 5\sqrt{\mathsf{Re}_x} & x < x_0 \\ 5\sqrt{\mathsf{Re}_{x_0}} + 0.16\left(\mathsf{Re}_x^{6/7} - \mathsf{Re}_{x_0}^{6/7}\right) & x > x_0 \end{cases} \tag{24-42}$$

By construction, this expression is continuous across the nominal transition point(see fig. 24.4).

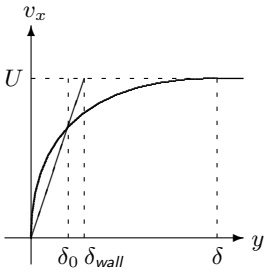

The "true" thickness δ_0 of the viscous sublayer is obtained from the intercept between Prandtl's power profile (24-37) and the linearly rising velocity in the sublayer. The kink at $y = \delta_0$ is unphysical, because it gives rise to a small jump in shear stress that violates Newton's third law (slightly). The real transition from viscous sublayer to turbulent main layer is softer than shown here.

The viscous sublayer

It is also possible to get an estimate of the thickness δ_0 of the viscous sublayer from the intercept between the linearly rising field, $v_x = y\bar{\sigma}_{\mathsf{wall}}/\eta$, in the sublayer and the power law (24-37). Demanding continuity at $y = \delta_0$, we get

$$\frac{\bar{\sigma}_{\mathsf{wall}}}{\eta}\delta_0 = U\left(\frac{\delta_0}{\delta}\right)^{1/7} \ .$$

Solving this equation for δ_0 and inserting σ_{wall} from (24-33) and δ from (24-41) we obtain[1]

$$\frac{U\delta_0}{\nu} = 206\mathsf{Re}_x^{1/42} \ . \tag{24-43}$$

At the nominal transition point $\mathsf{Re}_x = 5 \times 10^5$, this becomes 282, which grows to 337 at $\mathsf{Re}_x = 10^9$. The sublayer thickness is also plotted in Fig. 24.4 and its variation with Re_x is barely perceptible.

It is now also possible to calculate the fraction of the terminal velocity that the fluid has at the "edge" of the sublayer

$$\frac{v_x|_{y=\delta_0}}{U} = 2.8\mathsf{Re}_x^{-5/42} \ . \tag{24-44}$$

At the nominal transition point it is 0.59 and falls by roughly a factor 2 to 0.24 at $\mathsf{Re}_x = 10^9$.

[1] The remarkable 42'nd root may have deeper significance [48].

24.6 Boundary layers with varying slip-flow

In the two preceding sections we have only discussed the case of constant slip-flow, but now we turn to the study of slip-flows that vary with x. Although we shall always think of a flat plate boundary layer, the following discussion is also valid for slowly curving walls, such as the much-studied flow around a cylinder.

A varying slip-flow $U(x)$ will strongly influence the flow in the boundary layer (which we now again assume to be laminar). Accelerating flow ($dU/dx > 0$), tends to suppress the boundary layer, so that its downstream thickness grows slower than the $\sqrt{x}$ of the Blasius layer. Sufficiently strong acceleration may even make the boundary layer thinner downstream. Conversely, if the slip-flow decelerates ($dU/dx < 0$), the thickness will grow faster than $\sqrt{x}$, and sufficiently strong deceleration may lift the boundary layer off the plate and make it wander into the mainstream as a separated boundary layer.

In this section we shall establish some relations that are valid for any exact solution to Prandtl's equations. These relations will be useful for the discussion of the separation phenomenon to be taken up in the following sections.

Exact wall derivatives

At the wall, $y = 0$, we know that both v_x and v_y must vanish, and that the derivative of the velocity at the wall,

$$\omega = \left.\frac{\partial v_x}{\partial y}\right|_{y=0} \tag{24-45}$$

is in general non-vanishing, except at a separation point, where it has to vanish. We have used the letter ω to denote this quantity, because it has dimension of angular velocity. It should not be confused with the wall vorticity $\omega_z = -\omega$.

Setting $y = 0$ in the Prandtl equation (24-21) we get immediately the double derivative, also called the *wall curvature*,

$$\nu \left.\frac{\partial^2 v_x}{\partial y^2}\right|_{y=0} = -U\frac{dU}{dx} \ . \tag{24-46}$$

Its direct relation to the slip-flow opens for a qualitative discussion of the shape of the velocity profile. If the slip-flow accelerates ($dU/dx > 0$), the wall curvature will be negative and favor the approach of the velocity towards its terminal value, U. Conversely, if the slip-velocity decreases ($dU/dx < 0$), the wall curvature will be positive and adversely affect the approach to terminal velocity. This forces an inflection point into the velocity profile and raises the need for including higher derivatives to secure the turn-over towards the asymptotic slip-flow. For constant slip-flow, *i.e.* the Blasius case, we have $dU/dx = 0$, and the wall curvature vanishes.

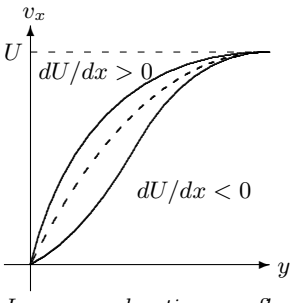

In accelerating flow, $dU/dx > 0$, the wall curvature is negative, whereas in decelerating flow the curvature is positive. The dashed curve sketches the velocity profile for vanishing wall curvature.

The higher order wall derivatives may be calculated by differentiating the Prandtl equation repeatedly after y. Differentiating once, we find

$$\nu \left.\frac{\partial^3 v_x}{\partial y^3}\right|_{y=0} = 0 \ , \tag{24-47}$$

and once more

$$\nu \left.\frac{\partial^4 v_x}{\partial y^4}\right|_{y=0} = \omega \frac{d\omega}{dx} \ . \tag{24-48}$$

Clearly, this process can be continued indefinitely to obtain all wall derivatives of v_x depending only on U and ω and their derivatives.

Exact integral relations

We have already derived a relation (24-36) from momentum balance in uniform flow. For general varying slip-flow we first rewrite the Prandtl equation (24-21) in the form,

$$-\nu \frac{\partial^2 v_x}{\partial y^2} = (U - v_x)\frac{dU}{dx} + \frac{\partial [v_x(U - v_x)]}{\partial x} + \frac{\partial [v_y(U - v_x)]}{\partial y} \ . \tag{24-49}$$

Integrating this equation over y from 0 to ∞, and using the boundary values $v_y \to 0$ for $y \to 0$ and $U - v_x \to 0$ for $y \to \infty$, we obtain the general von Kármán relation

$$\boxed{\nu \left.\frac{\partial v_x}{\partial y}\right|_{y=0} = \frac{dU}{dx}\int_0^\infty (U - v_x)\, dy + \frac{d}{dx}\int_0^\infty (U - v_x) v_x \, dy} \ . \tag{24-50}$$

It states that the drag on any infinitesimal slice of the plate equals the rate of momentum loss from the fluid.

We may similarly derive a relation expressing kinetic energy balance by multiplying the Prandtl equation with v_x, and rewriting it in the form,

$$\nu \left(\frac{\partial v_x}{\partial y}\right)^2 = \frac{1}{2}\nu \frac{\partial^2 (v_x^2)}{\partial y^2} + \frac{1}{2}\frac{\partial ((U^2 - v_x^2) v_x)}{\partial x} + \frac{1}{2}\frac{\partial (v_y (U^2 - v_x^2))}{\partial y} \tag{24-51}$$

Integrating this over all y and using the boundary conditions, we get

$$\boxed{\nu \int_0^\infty \left(\frac{\partial v_x}{\partial y}\right)^2 dy = \frac{1}{2}\frac{d}{dx}\int_0^\infty (U^2 - v_x^2) v_x \, dy} \ . \tag{24-52}$$

This relation states that the rate of heat dissipation in any infinitesimal slice equals the rate of loss of kinetic energy from the fluid. It is also possible to derive further relations for angular momentum balance and thermal energy balance [46].

Dynamic thicknesses

The integrands in the momentum and energy balance equations, (24-50) and (24-52), may be interpreted physically in terms of flow properties. The expression $U - v_x$ is the volume flux of fluid displaced by the plate, the expression $\rho_0(U-v_x)v_x$ is the flux of "lost momentum" caused by the presence of the plate, $\frac{1}{2}\rho_0(U^2-v_x^2)v_x$ is the flux of "lost kinetic energy", and $(\partial v_x/\partial y)^2$ is the density of heat dissipation.

It is convenient to introduce dynamic length scales (or thicknesses) related to each of these quantities (and the wall stress),

$$\frac{1}{\delta_{\mathsf{wall}}} = \frac{1}{U}\left.\frac{\partial v_x}{\partial y}\right|_{y=0} , \tag{24-53a}$$

$$\delta_{\mathsf{disp}} = \frac{1}{U}\int_0^\infty (U - v_x)\, dy , \tag{24-53b}$$

$$\delta_{\mathsf{mom}} = \frac{1}{U^2}\int_0^\infty (U - v_x)v_x\, dy , \tag{24-53c}$$

$$\delta_{\mathsf{ener}} = \frac{1}{U^3}\int_0^\infty (U^2 - v_x^2)v_x\, dy , \tag{24-53d}$$

$$\frac{1}{\delta_{\mathsf{heat}}} = \frac{1}{U^2}\int_0^\infty \left(\frac{\partial v_x}{\partial y}\right)^2 dy . \tag{24-53e}$$

In terms of these thicknesses, the momentum and energy balance equations now take the compact and quite useful forms,

$$\frac{\nu U}{\delta_{\mathsf{wall}}} = U\frac{dU}{dx}\delta_{\mathsf{disp}} + \frac{d\left(U^2\delta_{\mathsf{mom}}\right)}{dx} , \tag{24-54a}$$

$$\frac{\nu U^2}{\delta_{\mathsf{heat}}} = \frac{1}{2}\frac{d(U^3\delta_{\mathsf{ener}})}{dx} \tag{24-54b}$$

Again we emphasize that these relations, like the wall derivatives, must be fulfilled for any exact solution to Prandtl's boundary layer equations.

For the Blasius layer, self-similarity make all thicknesses proportional to the same basic scale, $\lambda = \sqrt{\nu x/U}$. Numeric integration yields,

$$\begin{aligned} &\delta_{\mathsf{wall}} \approx 3.012\,\lambda , \quad \delta_{\mathsf{disp}} \approx 1.721\,\lambda , \quad \delta_{\mathsf{mom}} \approx 0.664\,\lambda , \\ &\delta_{\mathsf{ener}} \approx 1.044\,\lambda , \quad \delta_{\mathsf{heat}} \approx 3.830\,\lambda , \qquad \delta_{99} \approx 4.910\,\lambda . \end{aligned} \tag{24-55}$$

The self-similarity thus guarantees that the ratios between any thicknesses are pure numbers independent of x. The integral relations (24-54) simplify in this case to,

$$\frac{1}{2}\delta_{\mathsf{wall}}\delta_{\mathsf{mom}} = \frac{1}{4}\delta_{\mathsf{heat}}\delta_{\mathsf{ener}} = \frac{\nu x}{U} . \tag{24-56}$$

These relations are of course fulfilled for the numeric values above.

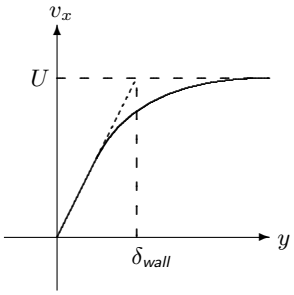

Definition of wall stress thickness from the intercept between the linearly rising velocity at small y and the mainstream velocity U.

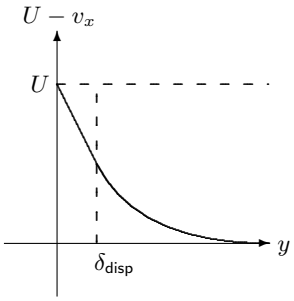

Definition of displacement thickness from the integral of the flux of volume loss, $U - v_x$.

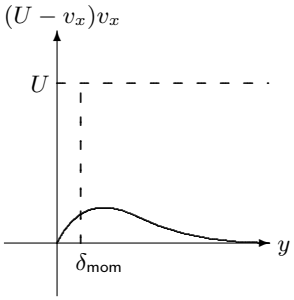

Definition of momentum thickness from the integral of the flux of momentum loss, $(U - v_x)v_x$.

24.7 Boundary layer separation

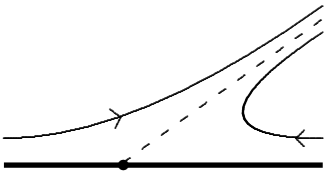

Schematic picture of how separation is thought to take place in a decelerating flow. The mainstream flow is profoundly changed by the separation both upstream and downstream from the separation point.

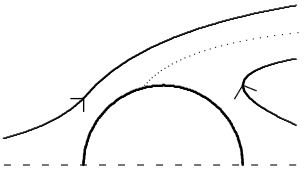

Sketch of the much-studied separation flow around a cylinder (of which only half is shown here). The separating streamline is dotted.

When a separating boundary layer takes off into a decelerating mainstream, the character of the mainstream flow is profoundly changed, thereby actually invalidating the Prandtl approximation. Careful analysis has revealed that this is a generic problem, to which the boundary layer equations respond by developing an unphysical singularity right at the point of separation. This *Goldstein singularity* [**?**] prevents us in general from using boundary layer theory to connect the regions before and after separation.

The existence of a singularity is nevertheless believed to be an indicator of boundary layer separation in the general vicinity of the point where the singularity occurs. During the 20'th century the problem of predicting the singular separation point for boundary layers around variously shaped objects has been of great importance to fluid mechanics, for fundamental as well as technological reasons. It has proven to be a challenging problem, to say the least [50]. A number of approximative schemes have been proposed and tried out, and with suitable empirical input, they compare reasonably well with analytic or numeric calculations [46].

The Goldstein singularity is unavoidable as long as we persist in the belief that we can employ Prandtl's equations and also specify the slip-flow velocity as we wish. The price to pay for avoiding the singularity is that the Prandtl equations must be replaced by the Navier-Stokes equations and that the mainstream flow cannot be fully specified in advance, but has to be allowed to be influenced by what happens deep inside the boundary layer. Since separation originates in the innermost viscous "deck" of the boundary layer, viscosity thus takes decisive part in selecting the presumed inviscid flow at large, again emphasizing that inviscid flow solutions are not unique, and that ideal flow is indeed — an ideal.

In the last half of the 20th century, it has been conclusively demonstrated through theoretical analysis and numerical simulation that the Navier-Stokes equations do not lead to any boundary layer singularities and do in fact smoothly connect the regions before and after separation. The successful method goes under the name "triple deck" because the boundary layer near the separation point is divided into three "decks" characterized by different physics and different length scales. Afterwards the decks are "stitched together" to make the complete boundary layer continuous. Although Prandtl's boundary layer theory strictly speaking is useless for separation problems, there does not seem to be any simple way of presenting the modern "interactive" boundary layer theory. We refer the reader to recent textbooks dedicated to the physics of boundary layers [50, 51].

In this section we shall make a — not particularly successful — attempt to determine the separation point from Prandtl's equations. The analysis demonstrates clearly the presence of a Goldstein singularity. In section 24.8 we shall see that empirical input is in fact not needed, and that it is possible to predict the position of the singularity to an accuracy better than 1%. A simplified but highly useful modification of this model yields an accuracy better than 3%.

	$U(x)$	x_c	wall	wall+mom	mom+ener	approx
1.	$1-x$	0.120	0.176	0.157	0.121	0.123
2.	$\sqrt{1-x}$	0.218	0.314	0.277	0.219	0.221
3.	$(1-x)^2$	0.064	0.094	0.084	0.064	0.065
4.	$(1+x)^{-1}$	0.151	0.230	0.214	0.154	0.158
5.	$(1+x)^{-2}$	0.071	0.107	0.098	0.072	0.074
6.	$1-x^2$	0.271	0.365	0.312	0.270	0.268
7.	$1-x^4$	0.462	0.565	0.491	0.460	0.449
8.	$1-x^8$	0.640	0.726	0.652	0.643	0.621
9.	$\cos x$	0.389	0.523	0.447	0.386	0.383

Table 24.1: *Table of decelerating slip-flows and the positions of their Goldstein singularities ("separation points") calculated in various models discussed in the text. The exact values x_c in the second column are taken from [46]. The separation points determined by the wall-anchored fourth order polynomial (24-57) are listed in the third column, and have typical errors of 40%. The fourth column is obtained by Pohlhausen's method (24-94) and errors less than 25% in all cases better than wall-anchored approximation. In the fifth column the separation points are determined from both momentum and energy balance (24-65) with typical errors smaller than 1%. Finally, in the last column, the separation points are derived from the simple approximation (24-75) with the typical error being less than 3%.*

Wall-anchored model

The simplest model of boundary layer flow is obtained by approximating the velocity profile with a fourth order polynomial in y constructed from the exact wall derivatives (page 425)

$$v_x = \omega\, y - \frac{U\dot{U}}{2\nu}\, y^2 + \frac{\omega\dot{\omega}}{24\nu}\, y^4 \ , \tag{24-57}$$

where a dot is used to denote differentiation after x. Evidently, this expression is exact for $y \to 0$, but for $y \to \infty$ where all three terms diverge, there is a problem. In decelerating slip-flow ($\dot{U} < 0$), the second order term is always positive, and the fourth-order term is always negative just upstream from the separation point, because the slope ω is positive and decreasing towards zero at separation. After an initial rise governed by the first and second order terms, the fourth order term must eventually pull down the profile to minus infinity, unless we manage to "catch" it at the top by requiring the value at maximum to be $v_x = U(x)$.

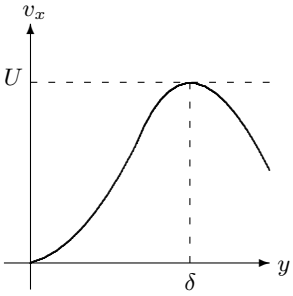

Wall-anchored fourth order polynomial joins continuously with $v_x = U$ at its maximum $y = \delta$. The continuation beyond δ drops to $-\infty$ in a decelerating slip-flow is unphysical.

This double condition determines both the slope ω and the thickness δ, but we do not have to solve this model in order to see that the separation point must be singular. For if the fourth order term should continue to "do its job" as we approach the separation point, it is necessary that $\omega\dot{\omega}$ be finite there, for example $2\omega\dot{\omega} = d(\omega^2)/dx = -\kappa^2$ with $\kappa > 0$. It then follows that close to the separation point we must have $\omega^2 = \kappa^2(x_c - x)$, or

$$\omega \approx \kappa\sqrt{x_c - x} \ . \tag{24-58}$$

Near the wall just upstream from the separation point, the velocity profile is

linear,

$$v_x \approx y\omega \approx \kappa y\sqrt{x_c - x}\ , \tag{24-59}$$

and from mass conservation (24-19) we determine the corresponding upflow

$$v_y \approx -\frac{1}{2}y^2\frac{d\omega}{dx} \approx \frac{\kappa}{4}\frac{y^2}{\sqrt{x_c - x}}\ . \tag{24-60}$$

Evidently, the upflow diverges for all y at the separation point. Apart from being totally unphysical, this shows that it is not possible to solve the separation problem within the Prandtl approximation itself, because one of the conditions for this approximation, $|v_y| \ll |v_x|$, fails miserably near the separation point.

The model is solved in problem 24.7 and the solution confirms the existence of the Goldstein singularity and provides a definite value for κ. The separation points obtained from this model are listed in the third column (marked "wall") in table 24.1 for nine decelerating slip-flows. They agree rather poorly with the exact results (second column), overshooting by up to 40%. The poor performance of the model must be ascribed to the much too solid anchoring of the boundary layer to the wall, which tends to generate large errors in the shape of the profile across the bulk of the boundary layer.

∗ 24.8 Locating the Goldstein singularity

Pohlhausen (19??).

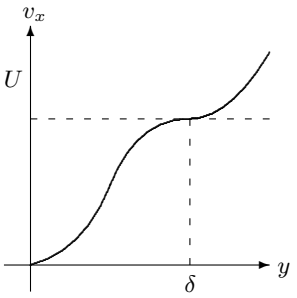

The fourth order polynomial joins smoothly with $v_x = U$ with a horizontal inflection point at $y = \delta$. The continuation beyond $y = \delta$ which diverges to $+\infty$ for $\mu < 3$ is not used.

The wall-anchored approximation (24-57) suffers from an unnatural jump in the curvature $\partial^2 v_x/\partial y^2$ at the edge of the boundary layer at $y = \delta$. A smoother fourth-order polynomial was introduced by Pohlhausen in 1921, in which the coefficients are fixed by demanding the field to approach $v_x = U$ at $y = \delta$ with vanishing first *and* second order derivatives. Parameterizing the polynomial with the dimensionless slope at the wall, it becomes

$$\frac{v_x}{U} = \mu\frac{y}{\delta} + 3(2-\mu)\left(\frac{y}{\delta}\right)^2 - (8-3\mu)\left(\frac{y}{\delta}\right)^3 + (3-\mu)\left(\frac{y}{\delta}\right)^4\ . \tag{24-61}$$

It contains two unknown functions: the dimensionless slope at the wall $\mu(x)$ and the layer thickness $\delta(x)$. One may readily verify that this indeed is $\mathcal{O}\left((y-\delta)^3\right)$ for $y \to \delta$.

Notice that for $\mu < 2$, the second and fourth order terms are always positive. It is the negative third order term, which secures the smooth turn-over towards the slip-flow at $y = \delta$. A selection of this family of profiles is shown in fig. 24.5. The profiles are well-defined for all μ, both before the separation point ($\mu > 0$) and after ($\mu < 0$). After separation they exhibit backflow, as one would expect, but as we shall see, the Goldstein singularity prevents us from connecting these solutions with the solutions before separation.

Pohlhausen solved the model by imposing the wall-curvature condition (24-46) together with the von Kármán relation (24-54a). The details are given in

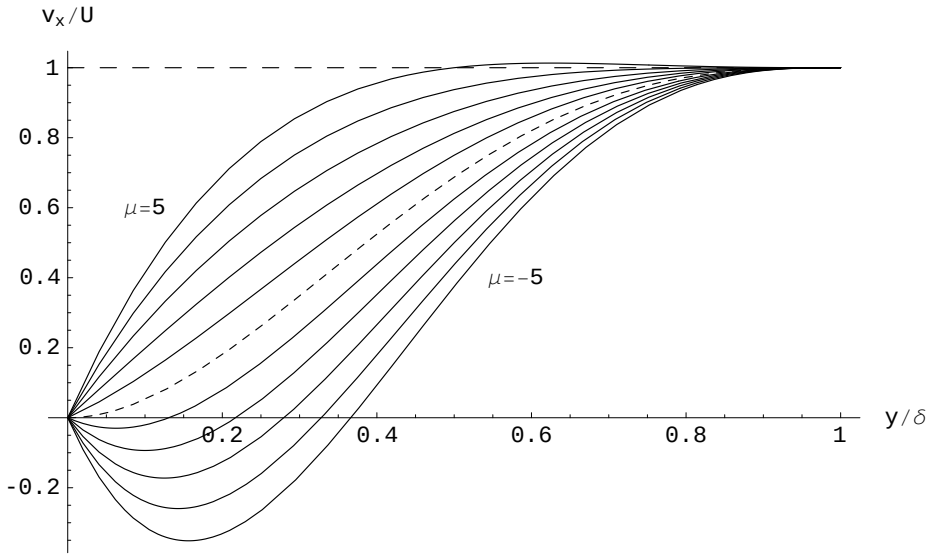

Figure 24.5: *Profiles of the Pohlhausen family for integer values of μ from -5 to +5. The dashed curve is the profile at separation, corresponding to $\mu = 0$, and the profiles with $\mu < 0$ have backflow.*

problem 24.8, and the separation point predictions are tabulated in the fourth column (marked "wall+mom") of table 24.1. The agreement is still rather poor with typical errors of 25%.

Momentum and energy balance

The nearly self-similar form of the Pohlhausen family (24-61), implies that all thicknesses are polynomials in μ scaled by δ. The wall, displacement, and momentum thicknesses become

$$\frac{\delta}{\delta_{\mathsf{wall}}} = \mu \ , \qquad \frac{\delta_{\mathsf{disp}}}{\delta} = \frac{8-\mu}{20} \ , \qquad \frac{\delta_{\mathsf{mom}}}{\delta} = \frac{144+12\mu-5\mu^2}{1260} \ . \tag{24-62}$$

and the energy and heat thicknesses,

$$\frac{\delta_{\mathsf{ener}}}{\delta} = \frac{10512+876\mu-253\mu^2-21\mu^3}{60060} \ , \qquad \frac{\delta}{\delta_{\mathsf{heat}}} = \frac{48-4\mu+3\mu^2}{35} \ . \tag{24-63}$$

Inserting these into the integral relations (24-54), one obtains two coupled first order differential equations for δ and μ.

These rather messy differential equations are simplified by means of the auxiliary variable

$$\gamma = \frac{\delta^2 U}{\nu} \ , \tag{24-64}$$

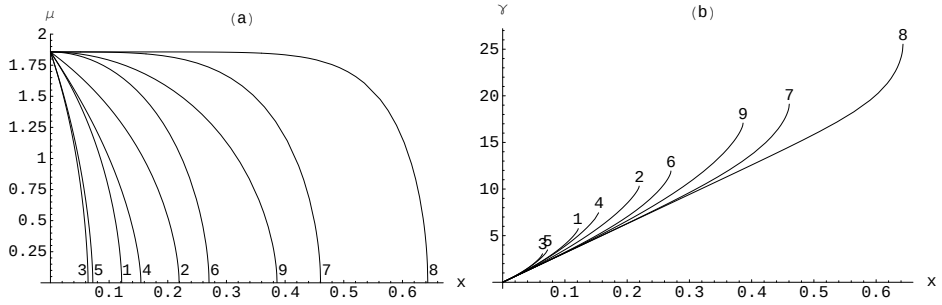

Figure 24.6: *Solutions to the coupled equations (24-65)for the nine fields in table (24.1).* **(a)** *The slope μ as a function of x. All curves have vertical tangent at the separation point, indicating a singularity.* **(b)** *The parameter γ defined in (24-64) as a function of x. The linear envelope $\gamma \approx 32\,x$ corresponds to the Blasius thickness $\delta \sim \sqrt{x}$.*

which has dimension of length. In these variables, one finds the still rather complicated equations,

$$4(6-5\mu)\gamma\dot{\mu} + (144+12\mu-5\mu^2)\dot{\gamma} + 15(96-6\mu-\mu^2)\gamma\frac{\dot{U}}{U} = 2520\mu \ , \quad \text{(24-65a)}$$

$$2(876-506\mu-63\mu^2)\gamma\dot{\mu} + (10512+876\mu-253\mu^2-21\mu^3)\left(\dot{\gamma}+5\gamma\frac{\dot{U}}{U}\right) = 6864(48-4\mu+3\mu^2) \quad \text{(24-65b)}$$

The boundary conditions are as before that $\delta = 0$ at the plate edge, $x = 0$, and this implies $\gamma(0) = 0$, but we must also know $\mu(0)$ to integrate the equations. Letting $\gamma \to 0$ in both differential equations, we can solve for the derivative $\dot{\gamma}(0)$ in two ways

$$\dot{\gamma}(0) = \frac{2520\mu}{144+12\mu-5\mu^2} = \frac{6864(48-4\mu+3\mu^2)}{10512+876\mu-253\mu^2-21\mu^3} \quad \text{(24-66)}$$

This fourth order algebraic equation for μ has four real roots, with the one closest to zero being

$$\mu(0) = 1.85685\ldots \ , \qquad \dot{\gamma}(0) = 31.3955\ldots \ . \quad \text{(24-67)}$$

The solutions are plotted in fig. 24.6 as function of x. One notices the vertical tangent of the slope at the separation point, indicating the presence of a Goldstein singularity. The calculated separation points are shown in the fifth column of table 24.1 and agree with the exact results to better than 1% in nearly all cases.

As a measure of how good the approximation really is, we calculate the error in satisfying the Prandtl equation,

$$\epsilon_x = v_x\frac{\partial v_x}{\partial x} + v_y\frac{\partial v_x}{\partial y} - U\frac{dU}{dx} - \nu\frac{\partial^2 v_x}{\partial y^2} \ . \quad \text{(24-68)}$$

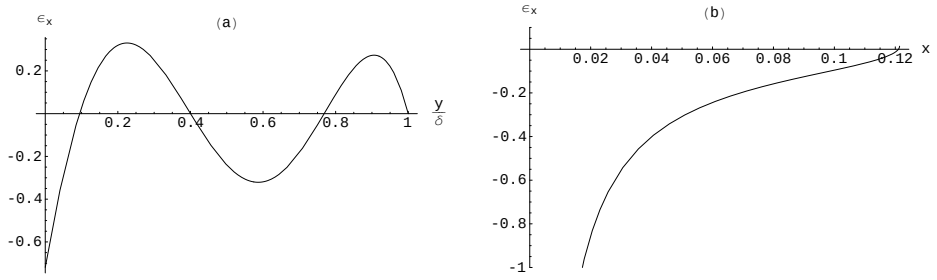

Figure 24.7: *The error field ϵ_x for the case $U = 1 - x$ calculated from eqs. (24-65).* **(a)** *The error field as a function of y/δ for $x = 0.6$.* **(b)** *The error field for $y = 0.5\delta$ as a function of x. One notices that the error is smallest close to the separation point $x = x_c = 0.121\ldots$, whereas it becomes quite large near the leading edge of the plate at $x = 0$.*

It plays the same role as a gravitational field, and the integral relations (24-54) then simply express that the total force and power of the error field must vanish for any slice of the boundary layer.

The error field is plotted for the case $U = 1 - x$ in fig. 24.7 as a function of y/δ for $x = 0.6$ and of x for $y/\delta = 0.5$. Although not particularly small compared to unity, the error oscillates with y/δ around zero because both the error force and power must vanish. The largest error is found near the leading edge of the plate at $x = 0$, where the Prandtl approximation anyway must break down. The smallest error is found near the separation point.

Approximative solution

Having established that the Pohlhausen family (24-61) yields precise values for the separation points when both momentum and energy balance are imposed, we now turn to the question of whether it is possible to simplify the model and still retain a reasonable predictive ability. Although the approximations below could also be made by manipulating the differential equations (24-65) directly, we prefer a more physical discussion in terms of the various thicknesses.

Multiplying the energy relation (24-54b) with $4U^3\delta_{\mathsf{ener}}$, we may rewrite it as

$$\frac{d(U^6\delta_{\mathsf{ener}}^2)}{dx} = 4\nu U^5 \frac{\delta_{\mathsf{ener}}}{\delta_{\mathsf{heat}}} \ . \tag{24-69}$$

The ratio between energy and heat thicknesses $\delta_{\mathsf{ener}}/\delta_{\mathsf{heat}}$ on the right hand side depends only on μ and is very nearly constant (close to 1/4) in the Pohlhausen model. As can be seen from fig. 24.8a, it varies only by about 12% in the whole interval $0 \le \mu \le 2$. Approximating the ratio $\delta_{\mathsf{ener}}/\delta_{\mathsf{heat}}$ by a perfect constant, we may immediately integrate the above equation to get,

$$U^6\delta_{\mathsf{ener}}^2 \approx 4\nu \frac{\delta_{\mathsf{ener}}}{\delta_{\mathsf{heat}}} \int_0^x U(x)^5\, dx \tag{24-70}$$

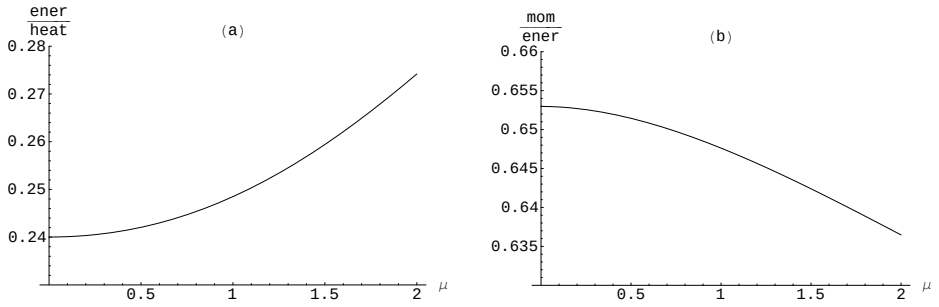

Figure 24.8: *Nearly constant thickness ratios in the Pohlhausen family.* **(a)** *The energy/heat ratio varies by about 12% between $\mu = 0$ and $\mu = 2$.* **(b)** *The momentum/energy ratio varies only by about 2.5% in the same interval.*

The integral defines a slip-flow length scale

$$L(x) = \frac{1}{U(x)^5} \int_0^x U(x)^5 \, dx \ , \tag{24-71}$$

which for constant slip-flow becomes $L(x) = x$. The energy relation may then be expressed as

$$\delta_{\mathsf{heat}} \delta_{\mathsf{ener}} = 4 \frac{\nu L(x)}{U(x)} \ , \tag{24-72}$$

which is of the same form as the Blasius result (24-56), although in this approximation it is generally valid.

The momentum equation (24-54a) is analogously multiplied with $2U^4\delta_{\mathsf{mom}}$, and rewritten in the form,

$$2\nu U^5 \frac{\delta_{\mathsf{mom}}}{\delta_{\mathsf{wall}}} = 2U^5 \dot{U} \left(\frac{\delta_{\mathsf{disp}}}{\delta_{\mathsf{mom}}} - 1 \right) \delta_{\mathsf{mom}}^2 + \frac{d(U^6 \delta_{\mathsf{mom}}^2)}{dx} \ . \tag{24-73}$$

The ratio of momentum to energy thicknesses $\delta_{\mathsf{mom}}/\delta_{\mathsf{ener}}$ is likewise a function of μ only in the Pohlhausen family. As seen from the plot in fig. 24.8b, it is very nearly constant (not far from to 2/3) and varies by only 2.5% in the interval $0 \le \mu \le 2$. If $\delta_{\mathsf{mom}}/\delta_{\mathsf{ener}}$ is assumed to be perfectly constant, we may use (24-69) to get the following algebraic relation between the various thicknesses

$$\frac{\delta_{\mathsf{mom}}}{\delta_{\mathsf{wall}}} = \frac{\dot{U} \delta_{\mathsf{mom}}^2}{\nu} \left(\frac{\delta_{\mathsf{disp}}}{\delta_{\mathsf{mom}}} - 1 \right) + 2 \frac{\delta_{\mathsf{mom}}^2}{\delta_{\mathsf{ener}} \delta_{\mathsf{heat}}} \ . \tag{24-74}$$

Neither of the ratios $\delta_{\mathsf{mom}}/\delta_{\mathsf{wall}}$ nor $\delta_{\mathsf{disp}}/\delta_{\mathsf{mom}}$ are constants as functions of μ.

At the separation point the wall stress vanishes so that $\delta_{\mathsf{mom}}/\delta_{\mathsf{wall}} = 0$. In the Pohlhausen family it follows from (24-62) that $\delta_{\mathsf{disp}}/\delta_{\mathsf{mom}} = 7/2$ for $\mu = 0$. Making use of (24-72) we obtain an equation that must be satisfied at the separation point

$$0 = 5 \frac{\dot{U} L}{U} + 1 \ .$$

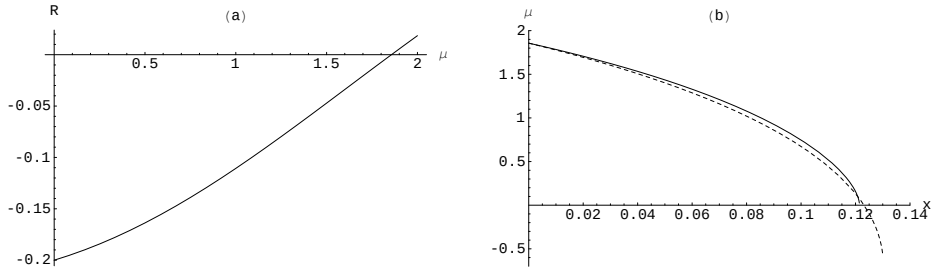

Figure 24.9: **(a)** *The right hand side of (24-76) as a function of μ.* **(b)** *The slope determined from (24-76) for the slip-flow $U = 1 - x$ (dashed line) compared with the solution to (24-65) (fully drawn). Notice that the Goldstein singularity has disappeared in the approximative solution, but that another singularity appears just beyond the separation point.*

More explicitly, the separation point must satisfy

$$\boxed{5U(x)^6 + \dot{U}(x) \int_0^x U(x)^5 \, dx = 0} \, . \tag{24-75}$$

The separation points obtained by solving this equation for the usual test cases are shown in the last column of table 24.1. The errors are typically less than 3%.

Recapitulating the derivation of this equation, the underlying input consists only in the constancy of $\delta_{\mathsf{ener}}/\delta_{\mathsf{heat}}$ and $\delta_{\mathsf{mom}}/\delta_{\mathsf{ener}}$, plus the value of $\delta_{\mathsf{disp}}/\delta_{\mathsf{mom}}$ at separation, all of which may be obtained from the Pohlhausen family (24-61). It is remarkable that a model as simple this can lead to so precise results. The explanation is presumably that even if the velocity profile does not solve the Prandtl equation particularly well everywhere (see fig. 24.7), it is nevertheless quite precise in the vicinity of the separation point. And it does satisfy both momentum and energy balance.

It is even possible to derive an approximative expression for the slope $\mu(x)$ by rewriting (24-74) in the form

$$\frac{\dot{U}(x)}{U(x)^6} \int_0^x U(x)^5 \, dx = \frac{\delta_{\mathsf{ener}}\delta_{\mathsf{heat}} - 2\delta_{\mathsf{mom}}\delta_{\mathsf{wall}}}{4\delta_{\mathsf{wall}}(\delta_{\mathsf{disp}} - \delta_{\mathsf{mom}})} \equiv R(\mu) \, . \tag{24-76}$$

The right hand side is a rational function of μ (for the Pohlhausen family) and may be solved numerically for μ given any x (see fig. 24.9b). Finally, $\delta(x)$ can be determined from (24-72).

The coarseness of the approximation makes the Goldstein singularity disappear, but that should not lead us to believe that it is meaningful to continue the model beyond the separation point, where μ crosses through zero. Anyway, another singularity appears just past the separation point, as may be seen from fig. 24.9b, which prevents any continuation beyond that point.

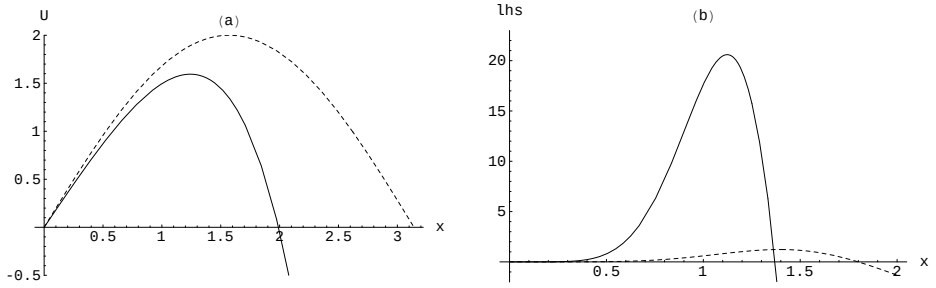

Figure 24.10: *Cylinder separation.* **(a)** *Potential slip-flow (dashed) and empirical fit (24-77).* **(b)** *The left hand side of (24-75) as a function of x for potential slip-flow (dashed) and empirical fit (24-77). Notice the steepness with which the zero is passed in the latter case.*

Separation from cylinder

Some of the more interesting slip-flows first accelerate and then decelerate. Among them the notorious cylinder in a uniform cross-wind, which has been the favorite target for boundary layer research during nearly a hundred years. The cylinder presents two difficulties, as does in fact every realistic separation problem. The first is the question of choosing the correct slip-flow. Since separation interacts with the mainstream flow, this is not so simple. The second is the technical question of calculating a precise value for the separation point in a slip-flow that may not purely decelerating.

If the external flow around the cylinder is taken to be potential flow, the slip-flow is given by (15-38), *i.e.* $U(x) = 2U_0 \sin x$ where U_0 is the strength of the uniform cross-wind and x is the angle of observation (the upwind direction corresponds to $x = 0$). It is harder to make the coupled differential equations (24-65) work in this case, whereas the approximative equation (24-75) immediately yields $x_c = 1.800 = 103°$. The exact numeric separation point for this slip-flow is known to be $x_c = 1.823 = 104°$ (see [46]), so in this case the approximation works to a precision only slightly worse than 1%.

The real flow around the cylinder is, however, not potential flow because of the vorticity induced into the main flow by the boundary layer, especially in the separation region and beyond. Hiemenz (1911) determined experimentally that the slip-flow at a Reynolds number $\mathsf{Re} = U_0 a/\nu = 9500$ was well described by the odd polynomial,

$$U = U_0(1.814x - 0.271x^3 - 0.0471x^5) \ . \qquad (24\text{-}77)$$

Now the approximative equation (24-75) predicts separation at $x_c = 1.372 = 78.6°$ which is about 2% away from the measured value $x_c = 80.5°$. Even if agreement is obtained, this is not very impressive, because the slip-flow itself has not been calculated from first principles. Most of the information about the separation from the cylinder lies in fact in the empirical slip-flow (see fig. 24.10).

Problems

24.1 a) Show that for constant slip-flow velocity it is possible to obtain a boundary layer of constant thickness on an infinitely extended plate, if fluid is sucked through the plate at a constant rate. b) Discuss what happens if fluid is pushed through instead.

∗ **24.2** Show that for a plate moving with velocity to $U(t)$ for $t > 0$ (and being at rest for $t < 0$) we have the general solution

$$v_x(y,t) = \int_0^t \left(1 - \operatorname{erf}\left(\frac{y}{2\sqrt{2\nu(t-t')}}\right)\right) \frac{dU(t')}{dt'}\, dt' \tag{24-78}$$

24.3 Show that for the Blasius solution

$$\int_0^\infty (1 - f(s))\, ds = h(\infty) \tag{24-79a}$$

$$\int_0^\infty f(s)(1 - f(s))\, ds = 2f'(0) \tag{24-79b}$$

24.4 Show that well outside the boundary layer but still close to the wall, the continuity equation (24-19) implies that

$$v_y(x,y) = \frac{dQ(x)}{dx} - y\frac{dU(x)}{dx}\ , \qquad \delta \ll y \ll L\ , \tag{24-80}$$

Interpret the two terms.

24.5 The form of the streamlines in Fig. 24.1 may be obtained directly from the Blasius solution. Show that

a) the streamlines are solutions to (with s given by (24-22))

$$\frac{dy}{dx} = \sqrt{\frac{\nu}{Ux}}\left(s - \frac{g(s)}{f(s)}\right) \tag{24-81}$$

b) this may be written

$$\frac{ds}{dx} = -\frac{1}{2x}\frac{g(s)}{f(s)} \tag{24-82}$$

c) a streamline satisfies

$$g(s) = \frac{C}{\sqrt{x}} \tag{24-83}$$

where C is a constant.

d) the explicit solution is

$$y = \sqrt{\frac{\nu x}{U}}\, g^{-1}\left(y_0\sqrt{\frac{U}{\nu x}}\right) \tag{24-84}$$

where g^{-1} is the inverse function of g, and y_0 the intercept with the y-axis.

∗ **24.6** Assume that a two-dimensional flow is of the form

$$v_x = U(x) \tag{24-85}$$

$$v_y = -y\frac{dU(x)}{dx} \tag{24-86}$$

all over space and not just near a boundary. Derive a third order differential equation for U and discuss its possible solutions.

Can one choose U freely if one adds $V(x)$ to v_y?

∗ **24.7** Consider the wall-anchored model (24-57).

a) Show that the polynomial has to satisfy the conditions

$$\omega - \frac{U\dot{U}}{\nu}\,\delta + \frac{\omega\dot{\omega}}{6\nu}\,\delta^3 = 0\ , \tag{24-87a}$$

$$\omega\,\delta - \frac{U\dot{U}}{2\nu}\,\delta^2 + \frac{\omega\dot{\omega}}{24\nu}\,\delta^4 = U\ , \tag{24-87b}$$

in order to reach maximum $v_x = U$ at $y = \delta$.

b) Show that there exists an algebraic relation between ω and δ,

$$\omega = \frac{4U}{3\delta}\left(1 + \frac{\dot{U}\delta^2}{4\nu}\right)\ , \tag{24-88}$$

c) Parameterize the model with a dimensionless slope μ,

$$\omega = \mu\frac{U}{\delta}\ , \qquad\qquad \delta = \sqrt{\frac{\nu(3\mu-4)}{\dot{U}}}\ . \tag{24-89}$$

d) Show that μ must satisfy the differential equation

$$\dot{\mu} = \frac{24}{\mu}\ \frac{2-\mu}{8-3\mu}\,\frac{\dot{U}}{U} - \mu\frac{4-3\mu}{8-3\mu}\left(2\frac{\dot{U}}{U} + \frac{\ddot{U}}{\dot{U}}\right)\ . \tag{24-90}$$

which should be solved with the initial condition $\mu(0) = 4/3$.

e) Show that close to separation the differential equation becomes

$$\mu\dot{\mu} \approx 6\frac{\dot{U}_c}{U_c}\ , \tag{24-91}$$

where $U_c = U(x_c)$ *etc.*

f) Show that there is a Goldstein singularity with

$$\kappa = -\dot{U}_c\sqrt{\frac{3U_c}{\nu}} \tag{24-92}$$

∗ **24.8** Consider the Pohlhausen family of velocity profiles (24-61).

a) Show that the wall-curvature condition implies that

$$\delta = \sqrt{\frac{6\nu(\mu-2)}{\dot{U}}} \ . \tag{24-93}$$

b) Show that the von Kármán relation leads to the differential equation

$$\dot{\mu} = 42\frac{48-20\mu+3\mu^2}{(4-\mu)(24+25\mu)}\frac{\dot{U}}{U} - (2-\mu)\frac{144+12\mu-5\mu^2}{(4-\mu)(24+25\mu)}\left(\frac{\ddot{U}}{\dot{U}} - 4\frac{\dot{U}}{U}\right) \ , \tag{24-94}$$

and integrate this equation numerically to obtain the separation points in the fourth column of table 24.1.

c) Is there a Goldstein singularity in this model?

